PAPER

Supporting coordination through hydrogen bonding in lanthanide complexes of 7-azaindole-*N*-oxide†

Oskar G. Wood, [iD] [a] Leanne Jones[b] and Chris S. Hawes [iD] *[a]

Ligands capable of simultaneous metal coordination and hydrogen bond donation provide useful structural features to enhance cooperativity and favour specific geometries within the coordination sphere. Here we present the first structurally characterised examples of coordination compounds containing protonated 7-azaindole-*N*-oxide **HL**, bearing a neutral oxo donor capable of terminal or bridging coordination modes adjacent to a convergent hydrogen bond donor. The ligand itself shows a strong tendency for dimeric assembly in the solid state, but is easily deprotonated to give the chelate complex [CuL₂] **1**. In the presence of lanthanide ions, however, four new complexes [Eu(NO₃)₃(HL)₃] **2**, [Gd(NO₃)₃(HL)₃] **3**, [Eu₂(μ₂-HL)₂(HL)₄-Cl₆] **4** and [YbCl₃(HL)₃][YbCl(HL)₅OH₂]2Cl **5** were prepared and crystallographically characterised. All four species show strong tendencies for hydrogen bonding from the ligand to impact their overall structures, including a C_3 propellor-like macrocyclic motif in **2** and **3** and a combination of intramolecular N–H···Cl contacts, and intermolecular tridentate anion binding in **5**. Solution studies including HRMS and phosphorescence emission spectroscopy reveal persistence of the europium complex **2** in solution, despite the multiple possible binding modes of this ligand, hinting at a degree of cooperativity in these systems. These results show the utility of hydrogen bonding within the coordination sphere for influencing structural outcomes, relevant to the construction of stable higher-order crystalline assemblies.

Introduction

In the design of supramolecular and metallo-supramolecular architectures, reversible and directional interactions such as hydrogen bonding provide a convenient intermediate level of structural influence, weaker than covalent and coordination bonds but more directional than other intermolecular forces.[1] A wide variety of extended networks have been prepared using hydrogen bonding as the main supramolecular driving force,[2] and intramolecular hydrogen bonds can also be used effectively within coordination assemblies to influence geometry, rigidity, and to help protect against ligand displacement.[3] This approach can be particularly effective in tuning the behaviour of metal binding pockets, for example in enhancing selectivity of metal extractions.[4] While amides and ureas are popular choices of hydrogen bond donors for supramolecular assemblies,[5]

heteroaromatic N–H functionalities provide a particularly rigid and directional hydrogen bond donor when incorporated into molecular assemblies.[6]

Where hydrogen bonding is desired alongside coordination bonding, pyrazole is a useful building block which combines a coordinating imine-like nitrogen atom directly attached to a pyrrole-like hydrogen bond donor.[7] N–H pyrazoles and indazoles have been widely used in engineering coordination polymers and MOFs supported by intra- or intermolecular hydrogen bonding,[8] with N–H···O contacts in particular playing a key role in mixed-ligand networks.[9] Beyond 1,2-diazoles however, endocyclic N–H donor functionality adjacent to a heterocyclic coordination site and with a sufficiently high pK_a to remain protonated under typical reaction and crystallisation conditions is less common. 7-Azaindole is one such example, containing a pyrrolic N–H donor fused to a pyridine ring as shown in Fig. 1. While well known in photophysical studies for its excited-state proton transfer behaviour and as a DNA base analogue,[10] the coordination chemistry of 7-azaindole and its derivatives has been somewhat less explored. Nonetheless, a small number of structurally characterised examples have shown the potential for this skeleton to form coordination compounds and multinuclear assemblies supported by coordination bonding, hydrogen bonding or both.[11]

[a] School of Chemical and Physical Sciences, Keele University, Keele ST55BG, UK.
E-mail: c.s.hawes@keele.ac.uk
[b] Faculty of Natural Sciences, Keele University, Keele ST55BG, UK

Fig. 1 The structures of 7-azaindole and 7-azaindole-*N*-oxide (**HL1**).

Fig. 2 Structure of a hydrogen-bonded dimer in the structure of **HL**, with heteroatom labelling scheme and hydrogen atoms shown in pink. Lattice solvent molecules and selected hydrogen atoms are omitted for clarity and ADPs are rendered at the 50% probability level.

Given the tendencies for heterocyclic *N*-oxides to form intricate high-connectivity coordination assemblies,[12] replacing the pyridine donor with a pyridine *N*-oxide would be anticipated to significantly diversify the possible coordination modes of 7-azaindole. If so, structure direction from ancillary hydrogen bonding would be an important asset in providing some level of structural control. Surprisingly, however, to date the only report examining the structural chemistry of 7-azaindole-*N*-oxide, either as an organic building block itself or in any coordination compounds, has been a contemporary report by Das and co-workers examining its role in copper-catalysed *N*-arylation reactions (*vide infra*).[13] Here, we explore 7-azaindole-*N*-oxide **HL** as a ligand capable of simultaneously coordinating to oxophilic lanthanide ions while facilitating hydrogen bonding to support the coordination sphere and influence the local and extended structure.

Results and discussion

Synthesis and structural characterisation

Based on the expected tendency for the ligand **HL** to coordinate a neutral *N*-oxide donor to one or more metal ions through the oxo group, we set out to build a picture of how coordination sphere hydrogen bonding impacts the local and extended structures of the resulting complexes. Firstly, single crystals of the free ligand were grown by slow evaporation from acetonitrile, to gauge the geometry and hydrogen bonding tendency in the absence of metal ions, and to compare with the ubiquitous 7-azaindole parent heterocycle.

The diffraction data were solved and refined in the monoclinic space group $P2_1/c$, revealing four crystallographically independent **HL** residues alongside three water molecules. Most likely, these water molecules arise from exposure to ambient air during evaporation. The N–O distances of all four residues are equivalent (1.3342(15)–1.3364(15) Å), comparable to that observed in typical pyridine *N*-oxides[14] and suggesting a similar donor strength. As shown in Fig. 2, while the hydrogen bonding interactions between molecules of **HL** take the form of dimers supported by $R_2^2(10)$ rings, similar to the $R_2^2(8)$ dimerization mode of substituted 7-azaindoles,[15] the lone pair geometry of the oxygen acceptors forces a cleft shape to the two molecules of each dimer. The mean interplanar angle of the two **HL** molecules involved in each dimer falls in the range 111–116°, while the N⋯O distances in the range 2.7018(16)–2.7714(16) imply relatively strong neutral hydrogen bonding interactions in these species. The lattice water molecules also engage in
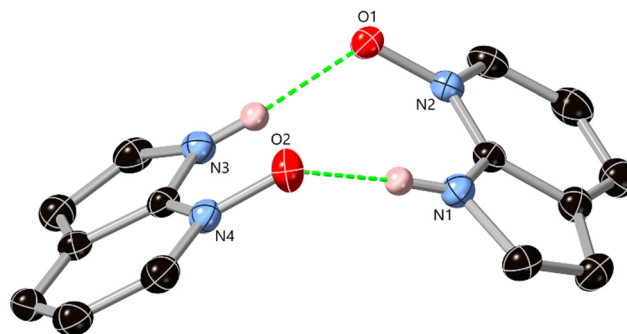
hydrogen bonding interactions. As well as H₂O⋯H₂O interactions, all four unique *N*-oxide oxygen atoms accept a second hydrogen bond from the lattice water molecules, although at a wider range of O⋯O distances (2.6845(15)–2.8146(15) Å). This tendency for *N*-oxide oxygen atoms to act as polytopic electron donors, capable of accepting up to three hydrogen bonds (or bridging up to three metal ions) is a key element of their importance as supramolecular tectons which differentiates and diversifies them from their parent heterocycles.[16] Recently, Das and co-workers reported the room-temperature structure of a triclinic hydrate of **HL** crystallised from dichloromethane/hexane, which exhibited similar angled hydrogen-bonded dimers between **HL** units.[13] Despite the less hydrophilic crystallisation solvent, association of water was still observed in that case, giving a hemihydrate **HL**·0.5H₂O.

The ligand **HL** was then combined with copper(II) acetate, initially with the aim of generating coordination compounds with a strongly hydrogen bond accepting anion. The only isolable phases from this reaction contained the deprotonated **L⁻** anion coordinating as a chelating ligand, indicating sufficient acidity from the N–H group to undergo deprotonation under these conditions. A recent study by Das and co-workers also observed direct deprotonation of **HL** on reaction of copper(II) fluoride in methanol in the absence of base.[13] The predominant phase [CuL₂] **1** is crystallised as green plates from methanol after combining with methanolic copper acetate at room temperature. In some batches, a minute quantity of a second blue phase was obtained, with the formula [Cu₂(OMe)₂L₂] (ESI†), but this phase was difficult to reproduce; both PXRD and elemental analysis confirmed that **1** is formed essentially exclusively under these conditions.

The diffraction data for **1** were solved and refined in the monoclinic space group $P2_1/n$ with the asymmetric unit containing the complex in its entirety, as shown in Fig. 3. The copper ion adopts a square planar, *trans* configuration with two **L** anions chelating. The Cu–N distances are shorter than the Cu–O distances (1.918(2) and 1.933(2) Å *versus* 1.997(2) and 2.011(2) Å, respectively), and the ligand enforces an average bite angle of 84.7°. On one face, a long axial Cu⋯O contact is evident at a distance of 2.5703(19) Å;
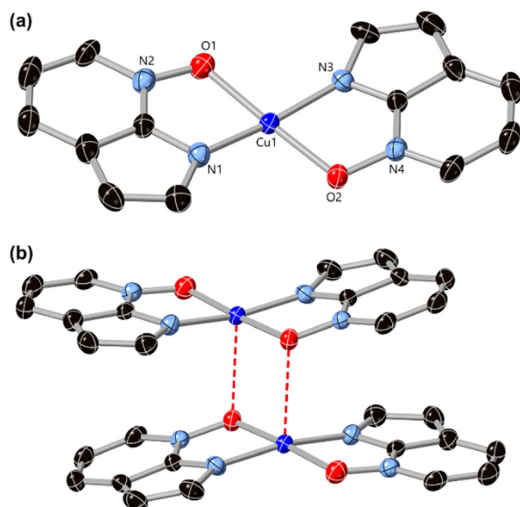
Fig. 3 (a) The structure of [Cu(L)₂] **1** with heteroatom labelling scheme. Hydrogen atoms are omitted for clarity and ADPs are rendered at the 50% probability level. (b) Contacts between adjacent complexes in the structure of **1**, where the oxo ligands weakly bridge *via* the axial coordination site of the adjacent copper ion.

Fig. 4 The structure of [Eu(NO₃)₃(**HL**)₃] **2** with labelling scheme for selected heteroatoms and hydrogen atoms shown in pink. Selected hydrogen atoms are omitted for clarity, and ADPs are rendered at the 50% probability level.

adjacent complexes dimerise through these contacts which are supported by offset face-to-face $\pi\cdots\pi$ interactions. The shortest interatomic distance in these interactions is 3.075(3) Å for N4···N1, though the two rings are bent outwards at an interplanar angle of 14.67(3)°. A second $\pi\cdots\pi$ contact is observed between parallel rings at a mean interplanar distance of 3.39 Å on the outer faces of the dimers, by which the dimers form a close-packed layer in the *ab* plane. Das and co-workers found that these dimeric species tend to be solvent dependent, and tended to observe a discrete CuL₂ complex crystallised from methanol (using copper(II) fluoride) and selective crystallisation of the axially-coordinated dimer **1** only when recrystallised from dichloromethane/hexane.[13] In our hands, using copper acetate as the copper source we observed only the axially bridged dimer and minute quantities of the methoxide bridged species.

While crystallisations were attempted with less basic anions of copper(II) in an attempt to preserve the acidic N–H functionality within the coordination sphere, we were unable to reproducibly isolate any other structurally-identifiable copper(II) complexes by this approach, in either methanol or acetonitrile as an aprotic alternative. Instead, we elected to focus our efforts on lanthanide ions, using chloride and nitrate anions and favouring acetonitrile except where this was impractical on solubility grounds for some lanthanide halides. Reaction of **HL** with europium(III) nitrate hexahydrate in acetonitrile at room temperature gave colourless crystals of [Eu(NO₃)₃(**HL**)₃] **2** after diffusion of diethyl ether vapour. The diffraction data, solved and refined in the triclinic space group $P\bar{1}$, revealed a 9-coordinate tricapped trigonal prismatic geometry for the europium ion with three monodentate **HL** species occupying one face and the remaining sites occupied by three chelating nitrato ligands, shown in Fig. 4. The **HL** oxygen atoms form shorter bonds to the europium ion (2.3295(11)–2.3566(13) Å)
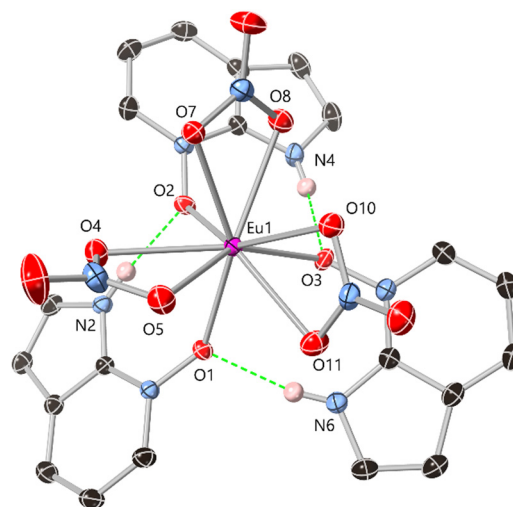
than the nitrato oxygen atoms (2.4522(13)–2.5321(13) Å), and all three show N–O–Eu angles in the range 132.61(8)–142.50(11)°.

Interestingly, the assembly of three **HL** species on the same face of the europium ion leads to a unique inner-sphere hydrogen bonding motif. As shown in Fig. 5, all three **HL** ligands accept and donate hydrogen bonds to adjacent ligands, forming a 15-membered $R_3^3(15)$ crown with a threefold propellor-like shape around the europium core. The N···O distances, in the range 2.7696(15)–2.822(2) Å are only marginally longer than those observed in the structure of the free ligand, indicating the acceptor capability of the *N*-oxide group is not significantly hindered by coordination. A similar hydrogen-bonded threefold propellor motif is observed in the Gd³⁺ complex of a 2-(*N*-amido)pyrimidine *N*-oxide ligand,
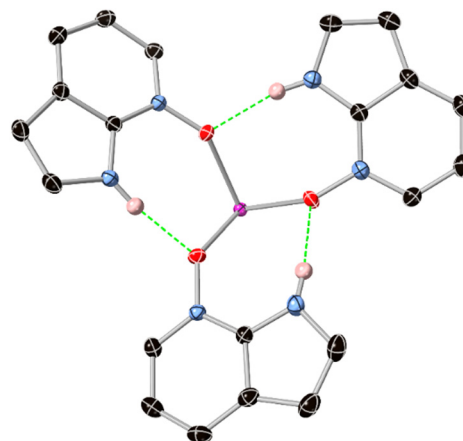

Fig. 5 Enlarged view of the M(**HL**)₃ assembly (M = Eu³⁺, Gd³⁺) in complexes **2** and **3** showing the hydrogen bonding fragment of the 15-membered ring surrounding one face of the metal ion. Selected hydrogen atoms are omitted for clarity; the ADPs are generated from the complex **2** model.

although in that case the steric bulk of a tetrathiafulvalene substituent forces much longer N⋯O distances (>2.98 Å).[17]

With all classical hydrogen bond donors occupied within the macrocyclic assembly, adjacent complexes of **2** associate through partially overlapped π⋯π interactions (although these are restricted somewhat by the propellor shape of the aromatic face of the complex) and more diffuse C–H⋯O contacts. Reaction of **HL** with gadolinium(III) nitrate in place of europium gave an isostructural complex [Gd(NO₃)₃(HL)₃] **3**, whose structural metrics were essentially equivalent. We were unable to generate crystalline material for structural analysis under the same conditions with either ytterbium or lanthanum nitrates, suggesting a cation size influence which may particularly favour intermediate lanthanide(III) ions for this assembly. If this apparent selectivity is maintained in the solution phase, such selectivity may contribute to a use for these complexes in lanthanide extraction and separation applications.

Carrying out a similar reaction between **HL** and europium(III) chloride in methanol also yielded colourless crystals following diffusion of diethyl ether vapour. The diffraction data, solved and refined in the triclinic space group $P\bar{1}$, revealed a centrosymmetric dimer of the form [Eu₂(μ₂-**HL**)₂(**HL**)₄Cl₆], as shown in Fig. 6. The two equivalent europium ions adopt 7-coordinate pentagonal bipyramidal coordination geometries with chlorido ligands occupying the two axial positions and one equatorial site. The remaining four coordination sites are occupied by oxygen atoms from **HL**, two in terminal positions and two bridging between the two europium ions. The Eu–Eu distance of 4.2727(5) Å is consistent with typical doubly *N*-oxido bridged Eu³⁺ species,[18] and unsurprisingly the bridging ligands show longer Eu–O distances than those in the terminal positions (2.430(2) and 2.509(2) Å, *versus* 2.268(2) and 2.327(2) Å). The latter are

shorter than those observed in complex **2**, due to the lower coordination number in **4**. The two bridging **HL** units exhibit disorder across two positions related by a 180° rotation about the vector bisecting the bridging Eu–O–Eu angle (ESI,† Fig. S8); similar disorder modes are regularly observed for ligands with mixed 6/5-membered rings and fused-ring systems.[19]

As all six **HL** units remain protonated, each acts as a hydrogen bond donor within the two coordination spheres. Unlike complexes **2** and **3**, however, only the chlorido ligands act as hydrogen bond acceptors. This can be rationalised by the bridging coordination mode of the central ligands occupying two of the three possible acceptor positions of these oxygen atoms, and the nearly opposite orientations of the two terminal ligands (with O1–Eu1–O2 angle of 168.1(3)°) restricting the possibility for inner-sphere N–H⋯O contacts. For the terminal sites, the N⋯Cl distances of 3.363(3) and 3.541(3) Å are typical for N–H⋯Cl contacts, though the smaller than ideal N–H⋯Cl angles of 167(4) and 137(3)°, respectively, suggests a mismatch in the bond lengths and angles within the rest of the $R_1^1(7)$ rings for ideal hydrogen bonding. The N–H groups of the two bridging **HL** species bisect two equivalent axial chlorido acceptors, with the second disordered orientation facing the equivalent situation on the opposite face of the molecule. Presumably, the presence of four chemically equivalent acceptors, and the lack of any significant directional interaction beyond these, relates to the tendency for disorder at this site. Adjacent complexes of **4** interact through various face-to-face π⋯π interactions in the *ac* plane, with face-to-face and edge-to-face interactions involving all six of the **HL** species from each complex. While X-ray powder diffraction shows the formation of a pure phase, the crystals are hygroscopic and showed slight association of atmospheric water on standing in air, exhibiting a tendency to clump together after standing in air, and displaying elemental analysis results more consistent with a partial hydrate.

Although a crystalline Yb(NO₃)₃ complex of **HL** was not forthcoming in our hands, reaction of **HL** with a sonicated dispersion of ytterbium chloride hexahydrate in acetonitrile followed by diethyl ether vapour diffusion gave colourless crystals of complex **5**. The diffraction data were solved and refined in the triclinic space group $P\bar{1}$, and revealed a salt of the formula [YbCl₃(**HL**)₃][YbCl(**HL**)₅OH₂]2Cl, shown in Fig. 7. The asymmetric unit contains two unique ytterbium sites. Yb1 is a seven-coordinate pentagonal bipyramidal species with five **HL** ligands occupying the equatorial positions, and axial positions filled by one chlorido and one aqua ligand. The **HL** ligands adopt a fivefold paddlewheel-like geometry around the central core, with three of the N–H groups on the same face as the aqua ligand and the remaining two facing the chlorido ligand. Yb2 adopts a *fac*-octahedral geometry defined by three chlorido ligands and three **HL** ligands. Two further non-coordinating chloride anions are present within the asymmetric unit, and although (as with the EuCl₃ complex **4**) the crystals appeared hygroscopic visually and by elemental analysis, no additional ordered lattice solvent was
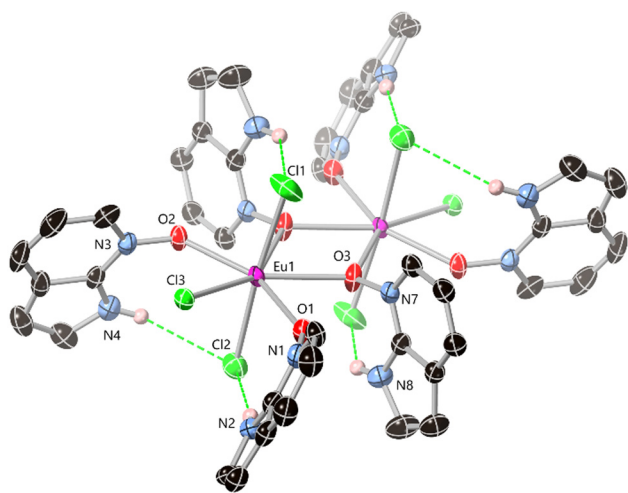

Fig. 6 Structure of complex [Eu₂(μ₂-**HL**)₂(**HL**)₄Cl₆] **4** with labelling scheme for unique heteroatoms and hydrogen atoms shown in pink. Selected hydrogen atoms are omitted for clarity and ADPs are rendered at the 50% probability level. Disorder on the O3 fragments is omitted for clarity (ESI,† Fig. S8).
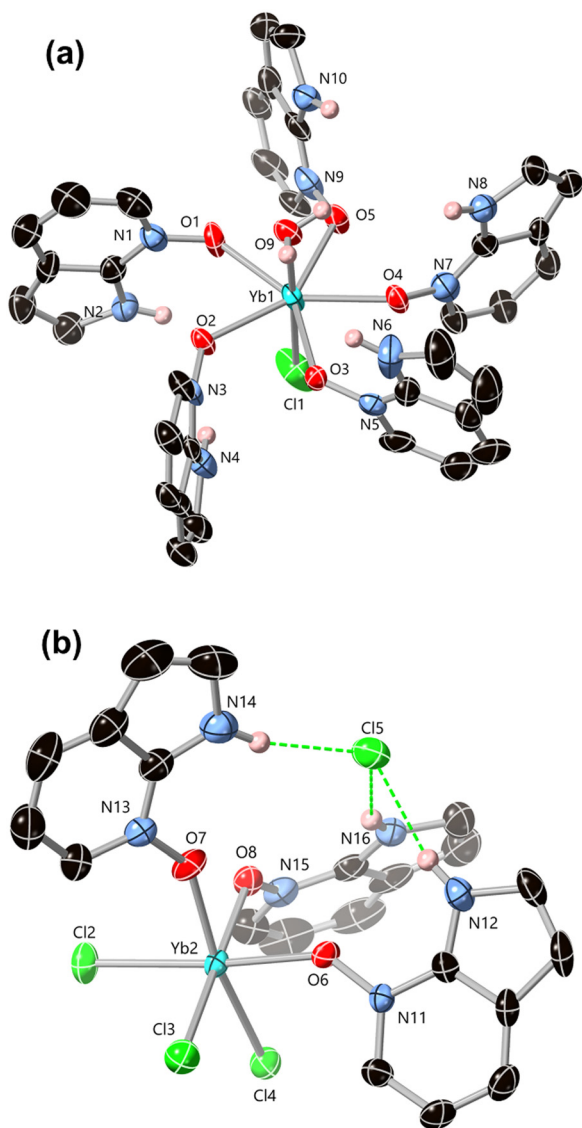
Fig. 7 The two Yb^{3+} environments in the structure of **5**, showing (a) the pentagonal bipyramidal coordination of Yb1 and (b) the octahedral environment of Yb2 and binding of a lattice chloride ion by tridentate hydrogen bonding from **HL**. Heteroatom labels are shown and hydrogen atoms are shown in pink. Selected hydrogen atoms and lattice anions are omitted for clarity. ADPs are rendered at the 50% probability level.

ring strain from the unbound chloride ion. The facially coordinated **HL** ligands attached to Yb2 each donate hydrogen bonds in a notable tris-chelate fashion to the other lattice chloride ion Cl5. The N···Cl distances in these interactions are shorter still, in the range 3.106(8)–3.149(6) Å, somewhat short for (sp^2) R_2N–H···Cl interactions with neutral donors and more comparable with charge-assisted contacts.[20] This suggests a potential for facially-coordinated **HL** species to act as anionophores, where similar chelate-type interactions have been put to good use in the outer coordination sphere for capturing anions.[21] Beyond classical hydrogen bonding, adjacent complexes interact through similar modes of π···π interaction as those observed in the other lanthanide complexes **2**–**4**.

Solution studies

The prevalence of inner-sphere hydrogen bonding in the complexes **2**–**4** prompted an investigation into the persistence of these species in solution, to establish whether these interactions furthered their stability beyond that expected of simple monodentate complexes. Electrospray ionisation mass spectrometry revealed that the $[M(NO_3)_3(HL)_3]$ motif (M = Eu, Gd) remains detectable in acetonitrile solution at low concentrations as the sodiated cations, and we could not identify any intermediate $[M(NO_3)_3(HL)_2]$ species. Similarly compound **1** was also readily detected as the protonated cation. We were unable to convincingly detect complex **4** or any likely fragments, while only the neutral octahedral species $[YbCl_3(HL)_3]$ from complex **5** was detected as the monosodiated cation; we were unable to detect the pentagonal bipyramidal dication or any likely fragments.

As the mass spectrometry results hinted at persistence of complexes **1**–**3** in solution, we employed photophysical measurements to probe the solution stability and likely speciation distribution of the complexes. We focused on the europium complexes **2** and **4**, based on the useful photophysical handle provided by the europium(III) phosphorescence emission which is readily sensitised by absorption from coordinated aromatic ligands.[22] The free ligand exhibits several absorbances below 350 nm in both acetonitrile and methanol, corresponding to various n → π* and/or π → π* transitions. Unlike the parent 7-azaindole,[23] only a single weak fluorescence band was observed with no significant solvent dependence, implying that the ESIPT processes involved in that system likely do not complicate interpretation of the spectra of the N-oxide complexes. The addition of aliquots of methanolic europium(III) chloride hexahydrate to a solution of **HL** in methanol failed to effect significant changes in the absorption spectrum, and no emergence of the characteristic Eu^{3+} phosphorescence bands was observed, suggesting minimal formation of complex **4** at photophysically-relevant concentrations in a competitive solvent and consistent with the HRMS results. However, titration of europium nitrate solution caused immediately

detected crystallographically, although the material gradually lost crystallinity after removal from the mother liquor.

Interestingly, and in contrast to complexes **2**–**4**, inner-sphere interactions are not the dominant mode of hydrogen bonding for the **HL** species in **5**. Only the two **HL** residues on Yb1 oriented towards the chlorido ligand donate hydrogen bonds within the coordination sphere, with N···Cl distances 3.305(7) and 3.908(8) Å similar to those in **4**. The other three **HL** species attached to Yb1, alongside the aqua ligand, donate hydrogen bonds to two symmetry equivalent sites of lattice chloride ion Cl6. The N···Cl distances in these interactions (3.195(9)–3.322(7) Å) are significantly shorter than the inner-sphere contacts, indicating a beneficial lack of
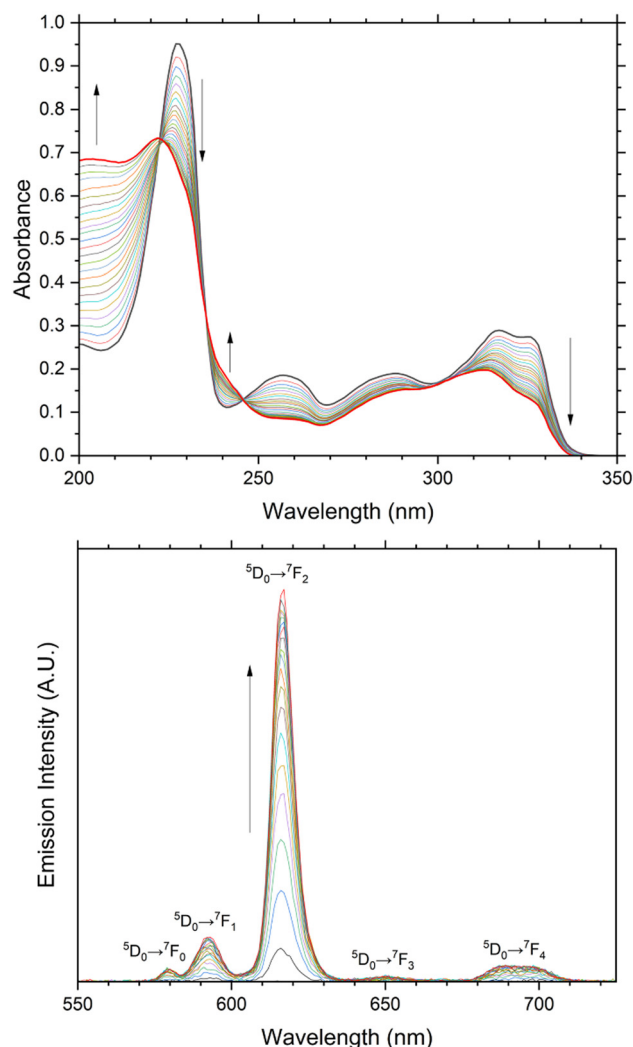
Fig. 8 Absorbance (top) and phosphorescence emission (bottom, λ_{ex} = 304 nm) spectra following sequential additions of Eu(NO₃)₃(H₂O)₆ aliquots (0 → 0.7 eq.) to **HL** (35 μM) in acetonitrile at room temperature.

visible changes in the absorbance profile of **HL** in acetonitrile, as shown in Fig. 8. The low energy ligand bands at 326 and 317 nm diminished with a stationary point slightly above 300 nm indicating growth of a new band in this region. The broad bands at 288 and 256 nm and the strong band at 227 nm also diminished with concurrent growth of a shoulder around 240 nm, and monotonic growth of a higher energy band at 203 nm corresponding to the free metal salt in solution.

In the phosphorescence emission spectra (Fig. 8), growth of the $^5D_0 \rightarrow {}^7F_J$ ($J = 0–4$) bands were observed with additions of Eu^{3+}, which gradually slowed after the 1M : 3L ratio was reached. The typically weak $^5D_0 \rightarrow {}^7F_0$ peak is clearly observed at 580 nm at 28% the intensity of the next $^5D_0 \rightarrow {}^7F_1$ band, fully consistent with the expected C_3 symmetry.[24] Global fitting of both the absorbance and phosphorescence spectra to a 1 : 3 binding model using Reactlab Equilibrium[25] gave an overall stability constant $\log\beta_3$ of 13.7(2), which gave

good fits to both sets of data without the need to model any other absorptive or emissive species in solution (ESI,† Fig. S11 and S12†). This value for the overall stability constant suggests only slightly lower stepwise stability constants for the **HL1**·Eu^{3+} system than for some Eu^{3+} complexes with neutral bidentate donors such as the well-known pyridyl-benzimidazole systems, at least in their mononuclear forms.[26] The phosphorescence decay profile was readily fitted to a monoexponential function with observed lifetime τ_{obs} = 0.24 ms (ESI,† Fig. S9). These data further support the existence of only a single sensitized Eu complex predominating in solution. The phosphorescence is relatively short-lived, consistent with the presence of multiple N–H oscillators within the inner coordination sphere,[27] particularly as these are engaged in hydrogen bonding with coordinated oxygen atoms. Based on the combined structural, HRMS and photophysical data, we suggest the pseudo-macrocyclic motif observed crystallographically is also predominant in solution for complex **2**, which seems to exhibit a cooperative binding process supported by hydrogen bonding to favour the 1M : 3L complex.

Experimental

Synthesis of [CuL₂] 1

To a solution of **HL** (10 mg, 75 μmol) in methanol (5 mL) was added a solution of copper(II) acetate hydrate (15 mg, 75 μmol) in methanol (5 mL). The resulting green solution was sealed and allowed to stand undisturbed for 48 hours, depositing dark green crystals of the product which were isolated by filtration and washed with cold methanol. A trace quantity of the blue phase [Cu₂(OMe)₂L₂] (ESI†) is occasionally observed in this preparation but bulk characterisation shows this phase is not present in significant quantities. Yield 7 mg (21 μmol, 57%). MP 263–265 °C (decomp.); found C, 50.60; H, 3.07; N, 16.76%; calculated for C₁₄H₁₀N₄O₂Cu C, 50.99; H, 3.06, N, 16.99%; m/z 330.0168 ([M + H]⁺, calculated for C₁₄H₁₁CuN₄O₂ 330.0178); ν_{max} (ATR, cm⁻¹) 3078m sh, 1596m, 1489s, 1469m, 1445m, 1384m, 1343s, 1312m, 1251m, 1222s, 1176m, 1152s, 1040m, 947m, 860m, 794m, 781s, 720s, 689s.

Synthesis of [Eu(NO₃)₃(HL)₃] 2

To a solution of **HL** (20 mg, 150 μmol) in acetonitrile (5 mL) was added a solution of europium(III) nitrate hexahydrate (24 mg, 54 μmol) in acetonitrile (5 mL). The resulting solution was briefly sonicated to ensure full dissolution, and then subjected to diffusion of diethyl ether vapour. After 1 week, colourless single crystals of the product were recovered by filtration. Yield 17.9 mg (24 μmol, 48%). MP 214–217 °C; found C, 33.96; H, 2.43; N, 17.06%; calculated for C₂₁H₁₈N₉O₁₂Eu C, 34.07; H, 2.45; N, 17.03%; m/z 764.0213 ([M + Na]⁺, calculated for C₂₁H₁₈EuN₉O₁₂Na 764.0185); ν_{max} (ATR, cm⁻¹) 3149w, 3098m sh, 2927w sh, 1626w, 1499s, 1461s, 1424m, 1349m, 1331m, 1283s, 1246s, 1227s, 1171m, 1109w, 1046m, 1025m, 958w, 897w, 860m, 789s, 698s sh.

Synthesis of [Gd(NO$_3$)$_3$(HL)$_3$] 3

The preparation of the title compound was equivalent to compound **2**, using gadolinium(III) nitrate hexahydrate (24 mg, 53 μmol) in place of europium. Yield 26.8 mg (36 μmol, 72%). MP 217–219 °C; found C, 33.92; H, 2.42; N, 16.62%; calculated for C$_{21}$H$_{18}$N$_9$O$_{12}$Gd C, 33.83; H, 2.43; N, 16.91%; *m/z* 769.0227 ([M + Na]$^+$, calculated for C$_{21}$H$_{18}$GdN$_9$O$_{12}$Na 769.0214); v_{max} (ATR, cm^{-1}) 3139w, 3098m sh, 2925w sh, 1622w, 1461s sh, 1349s, 1283s, 1246s, 1228s, 1173m, 1108m, 1062w, 1044m, 1024m, 961w, 859m, 788s, 741m, 700s sh, 614m, 597m.

Synthesis of [Eu$_2$(μ$_2$-HL)$_2$(HL)$_4$Cl$_6$] 4

To a solution of **HL** (20 mg, 150 μmol) in methanol (3 mL) was added a solution of europium(III) chloride hexahydrate (22 mg, 60 μmol) in methanol (3 mL). The solution was briefly sonicated and subjected to diffusion of diethyl ether vapour, yielding colourless crystals of the title compound within one week which were isolated by filtration. The crystals readily associated with atmospheric water on standing in air. Yield 10.7 mg (8.1 μmol, 32%). MP 266–271 °C (decomp.); found C, 36.85; H, 2.68; N, 11.91%; calculated for C$_{42}$H$_{36}$N$_{12}$O$_6$Cl$_6$Eu$_2$ + 3H$_2$O C, 36.67; H, 3.08; N, 12.22%; v_{max} (ATR, cm^{-1}) 3193m br, 3093m, 1622m br, 1497s, 1457s, 1423m, 1350s, 1332s, 1288m, 1243s, 1225m, 1169m, 1099w, 1037s, 964w, 858m, 788s, 712s.

Synthesis of [YbCl$_3$(HL)$_3$][YbCl(HL)$_5$OH$_2$]2Cl 5

A solution of **HL** (20 mg, 150 μmol) in acetonitrile (4 mL) was added to a suspension of ytterbium(III) chloride hexahydrate (12 mg, 31 μmol) dispersed in acetonitrile (6 mL). The resulting suspension was sonicated for 5 minutes and filtered, and the filtrate was subjected to diffusion of diethyl ether vapour. After one week, colourless crystals were isolated by filtration. Similarly to complex **4**, this solid also readily adsorbs atmospheric water, and loses crystallinity on extended air exposure. Yield 7.6 mg (4.6 μmol, 30%). MP 186–190 °C (decomp.); found C, 37.06; H, 3.09; N, 11.99%; calculated for C$_{56}$H$_{50}$N$_{16}$O$_9$Cl$_6$Yb$_2$ + 8H$_2$O C, 37.49; H, 3.71; N, 12.49%; *m/z* 703.9787 (octahedral species [M + Na]$^+$, calculated for C$_{21}$H$_{18}$Cl$_3$N$_6$O$_3$YbNa 703.9792); v_{max} (ATR, cm^{-1}) 3190s br, 3082m, 1621m br, 1499s, 1456s, 1423m, 1349s, 1330s, 1285w, 1244s sh, 1222m, 1169m, 1105w, 1035m, 891w, 858m, 790s, 712s.

Conclusions

The 7-azaindole-*N*-oxide ligand **HL** provides a convenient and pre-organized source of hydrogen bonding to structurally influence the inner coordination sphere in lanthanide complexes. While this group is readily deprotonated in the presence of copper(II) salts, in lanthanide complexes these hydrogen bonds appear to buttress the coordination environment. In complexes **2** and **3**, a 15-membered C_3-symmetric cyclic hydrogen bonding motif encircles the metal

ion, and spectroscopic evidence suggests that this species forms cooperatively and persists in solution. Complexes **4** and **5** show diverse coordination and hydrogen bonding modes of the **HL** ligand. Both bridging and terminal coordination behaviour is seen in complex **4**, while the mixed coordination numbers of the two Yb^{3+} fragments in complex **5** also exhibit both inter- and intra-molecular hydrogen bonding in the crystalline phase. These results indicate that combined coordination and hydrogen bonding assemblies of 7-azaindole-*N*-oxide and its analogues may be powerful structural motifs for designing higher order crystalline assemblies, using hydrogen bonding as a handle for reinforcing the otherwise labile coordination behaviour of *N*-oxide ligands.

Author contributions

OGW: conceptualization, investigation, writing. LJ: investigation, formal analysis, writing. CSH: conceptualization, investigation, supervision, writing.

Conflicts of interest

There are no conflicts to declare.

Acknowledgements

References

1 L. J. Karas, C.-H. Wu, R. Das and J. I.-C. Wu, *WIREs Comput. Mol. Sci.*, 2020, **10**, e1477.

2 R.-B. Lin and B. Chen, *Chem*, 2022, **8**, 2114–2135; D. A. Cullen, M. G. Gardiner and N. G. White, *Chem. Commun.*, 2019, **55**, 12020–12023; Y.-L. Li, E. V. Alexandrov, Q. Yin, L. Li, Z.-B. Fang, W. Yuan, D. Proserpio and T.-F. Liu, *J. Am. Chem. Soc.*, 2020, **142**, 7218–7224; P. Li, M. R. Ryder and J. F. Stoddart, *Acc. Mater. Res.*, 2020, **1**, 77–87.

3 C. S. Hawes, *Dalton Trans.*, 2021, **50**, 6034–6049.

4 R. S. Forgan, B. D. Roach, P. A. Wood, F. J. White, J. Campbell, D. K. Henderson, E. Kamenetzky, F. E. McAllister, S. Parsons, E. Pidcock, P. Richardson, R. M. Swart and P. A. Tasker, *Inorg. Chem.*, 2011, **50**, 4515–4522; J. R. Turkington, P. J. Bailey, J. B. Love, M. Wilson and P. Tasker, *Chem. Commun.*, 2013, **49**, 1891–1899.

5 C. Kulkarni, E. W. Meijer and A. R. A. Palmans, *Acc. Chem. Res.*, 2017, **50**, 1928–1936; A. E. Hooper, S. R. Kennedy, C. D. Jones and J. W. Steed, *Chem. Commun.*, 2016, **52**, 198–201; O. Kotova, R. Daly, C. M. G. dos Santos, M. Boese, P. E. Kruger, J. J. Boland and T. Gunnlaugsson, *Angew. Chem., Int. Ed.*, 2012, **51**, 7208–7212; R. Wechsel, M. Žabka, J. W. Ward and J. Clayden, *J. Am. Chem. Soc.*, 2018, **140**, 3528–3531.

6 D. A. Leigh, C. C. Robertson, A. M. Z. Slawin and P. I. T. Thomson, *J. Am. Chem. Soc.*, 2013, **135**, 9939–9943; G. I. Vargas-Zúñiga and J. L. Sessler, *Coord. Chem. Rev.*, 2017, **345**, 281–296.

7 M. A. Halcrow, *Dalton Trans.*, 2009, 2059–2073.

8 S. Milan, G. Makhloufi and C. Janiak, *Z. Anorg. Allg. Chem.*, 2019, **645**, 893–899; S. Sengupta, S. Ganguly, A. Goswami, S. Bala, S. Bhattacharya and R. Mondal, *CrystEngComm*, 2012, **14**, 7428–7437; C. S. Hawes and P. E. Kruger, *Dalton Trans.*, 2014, **43**, 16450–16458.

9 T. Basu, H. A. Sparkes, M. K. Bhunia and R. Mondal, *Cryst. Growth Des.*, 2009, **9**, 3488–3496.

10 R. S. Moog and M. Maroncelli, *J. Phys. Chem.*, 1991, **95**, 10359–10369; A. V. Smirnov, D. S. English, R. L. Rich, J. Lane, L. Teyton, A. W. Schwabacher, S. Luo, R. W. Thornburg and J. W. Petrich, *J. Phys. Chem. B*, 1997, **101**, 2758–2769.

11 A. Domínguez-Martín, M. D. P. Brandi-Blanco, A. Matilla-Hernández, H. El Bakkali, V. M. Nurchi, J. M. González-Pérez, A. Castiñeiras and J. Niclós-Gutiérrez, *Coord. Chem. Rev.*, 2013, **257**, 2814–2838; A. B. Coles, O. G. Wood and C. S. Hawes, *J. Serb. Chem. Soc.*, 2023, DOI: **10.2298/ JSC230623061C**, In Press.

12 Y. Xiong, Y.-Z. Fan, R. Yang, S. Chen, M. Pan, J.-J. Jiang and C.-Y. Su, *Chem. Commun.*, 2014, **50**, 14631–14634; S. J. Bullock, L. P. Harding, M. P. Moore, A. Mills, S. A. F. Piela, C. R. Rice, L. Towns-Andrews and M. Whitehead, *Dalton Trans.*, 2013, **42**, 5805–5811.

13 K. Mondal, N. Mukhopadhyay, S. Patra, T. Roy and P. Das, *ACS Catal.*, 2023, **13**, 11977–11995.

14 D. Ülkü, B. P. Huddle and J. C. Morrow, *Acta Crystallogr., Sect. B: Struct. Sci., Cryst. Eng. Mater.*, 1971, **27**, 432–436.

15 B. Marzyk-Ociepa, K. Dysz, I. Turowska-Tyrk and D. Michalska, *J. Mol. Struct.*, 2015, **1101**, 91–100.

16 R. Puttreddy and P. J. Steel, *CrystEngComm*, 2014, **16**, 556–560.

17 F. Pointillart, Y. Le Gal, S. Golhen, O. Cador and L. Ouahab, *Inorg. Chem.*, 2009, **48**, 4631–4633.

18 Z. Wang, N. Liu, H. Li, P. Chen and P. Yan, *Eur. J. Inorg. Chem.*, 2017, 2211–2219; L. Armelao, D. B. Dell'Amico, L. Bellucci, G. Bottaro, S. Ciattini, L. Labella, G. Manfroni, F. Marchetti, C. A. Mattei and S. Samaritani, *Eur. J. Inorg. Chem.*, 2018, 4421–4428; F. Pointillart, B. Le Guennic, O. Maury, S. Golhen, O. Cador and L. Ouahab, *Inorg. Chem.*, 2013, **52**, 1398–1408.

19 A. T. Baker, N. J. Ferguson, H. A. Goodwin and A. D. Rae, *Aust. J. Chem.*, 1989, **42**, 623–638; J. W. Goodwin, P. E. Kruger and C. S. Hawes, *J. Coord. Chem.*, 2021, **74**, 341–360.

20 T. Steiner, *Acta Crystallogr., Sect. B: Struct. Sci., Cryst. Eng. Mater.*, 1998, **54**, 456–463.

21 S. H. Hewitt, G. Macey, R. Mailhot, M. R. J. Elsegood, F. Duarte, A. M. Kenwright and S. J. Butler, *Chem. Sci.*, 2020, **11**, 3619–3628.

22 B. Alpha, R. Ballardini, V. Balzani, J.-M. Lehn, S. Perathoner and N. Sabbatini, *Photochem. Photobiol.*, 1990, **52**, 299–306.

23 C. A. Taylor, M. A. El-Bayoumi and M. Kasha, *Proc. Natl. Acad. Sci. U. S. A.*, 1969, **63**, 253–260; J. Konijnenberg, A. H. Huizer and C. A. G. O. Varma, *J. Chem. Soc., Faraday Trans. 2*, 1988, **84**, 1163–1175.

24 K. Binnemans, *Coord. Chem. Rev.*, 2015, **295**, 1–45.

25 *ReactLab Equilibria*, Jplus Consulting Ltd, Fremantle, Australia, 2018.

26 J. Hamacek, S. Blanc, M. Elhabiri, E. Leize, A. Van Dorsselaer, C. Piguet and A.-M. Albrecht-Gary, *J. Am. Chem. Soc.*, 2003, **125**, 1541–1550.

27 R. M. Supkowski and W. D. Horrocks Jr., *Inorg. Chim. Acta*, 2002, **340**, 44–48.